An Approach To The Impedance Modelling of Low-Voltage Cables in Digital Twins

Rémy Cleenwerck[a,b,*], Hakim Azaioud[a], Robbert Claeys[a], Thierry Coosemans[b], Jos Knockaert[a], Jan Desmet[a]

[a] *EELab/Lemcko, Universiteit Gent, Graaf Karel de Goedelaan 34, 8500, Kortrijk, Belgium*
[b] *EVERGi Research Group, MOBI, Vrije Universiteit Brussel, Pleinlaan 2, 1050, Brussels, Belgium*

Abstract

The volatility of distributed production and the uncoordinated charging of electric vehicles cause major challenges in terms of supply reliability and local congestion problems in the distribution networks. In order to tackle these two aspects preventively, digital twin models are introduced to analyse the impacts of these stochastic distributed grid exchanges. Herein, line impedances are a key feature which determines the accuracy of the model. The chosen software environment to set up these digital twins, is based on Carson's equations which are typically used for overhead high voltage lines. Hence, in this contribution an adapted model of Carson's equations on low-voltage underground cables at 50 Hz is presented, with the aim to develop a digital twin for analysing the integration of nowadays loads and distributed sources on low voltage distribution systems. Finally, the model will be validated based on realistic grid and smart meter data provided by a distribution system operator.

Keywords: Low-voltage distribution systems, Impedance modelling, Cable geometry, Digital twin modelling

1. Introduction

In order to meet the EU-targets (cf. 'Fit-for-55 package' and the COP26 goals, e.g., speed up the roll-out of electric vehicles) a green wave of investments towards renewable energy sources and e-mobility is required. Existing low-voltage distribution systems (LVDS) are often not designed for this purpose and consequently do face serious challenges in the coming years. The emerging need for the estimation of the local hosting capacity in low-voltage (LV) grids caused by (i) the integration of renewable energy sources (RES) and (ii) the implementation of charging infrastructure for electric vehicles, becomes a necessity. A typical approach for simulating this, is by using digital twins to explore different scenarios. Digital twin environments such as OpenDSS and PowerFactory rely on Carson's equations [1]. Herein, it was observed in the literature that the application of the modified equations [2] was applied without adaptation for the purpose of the investigated low-voltage distribution network. For example, in [3] and [4] the authors use the modified equations, neglecting the boundary conditions who has to be fulfilled to employ them. Therefore, the performance of the modified Carson's equations is studied within this paper.

Although simulations are often carried out for high-voltage grids, the complexity for modelling LV distribution grids increases, since LVDS all over Europe can be completely different. Starting from the exploitation methods, over network configurations up to different cable topologies, etc. As a result, a generic approach to network studies using standard models as the 'IEEE European Low-Voltage test feeder' [5] as analysed in [6], cannot be applied.

In the UK which forms the basis of the 'IEEE European Low Voltage test feeder' model, a grounded neutral is applied. While in Belgium or Germany, the neutral conductor is not earthed as demonstrated by Lacroix et al. [7]. The latter is connected to the ground only at the star point of the LV distribution transformer. Depending on how the earthing system is operated, either a (i) TT- or a (ii) TN-earthing system is obtained. In the first case (i), the earth conductor does not run to the end user and therefore the end user has a separate earthing (Fig. 1). Additionally, the earthing remains separate from the neutral conductor at the load. The discrepancy between the different grids is discussed in the next section.

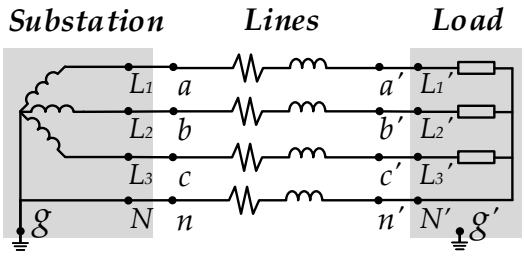

Figure 1: Equivalent circuit of TT-earthing system

*Corresponding author.
Email address: Remy.Cleenwerck@UGent.be (Rémy Cleenwerck)

The contributions of this paper are:

1. The discrepancy caused by applying the modified Carson's equations to low-voltage distribution networks where other boundary conditions are applicable is studied.
2. Investigation of the consequences, in terms of voltage deviation, that a simplified model of the cable geometry imposes compared to the modelling of the different cable designs (i.e., round, sector-shaped, solid and stranded core).
3. Numerical validation of the proposed method using a realistic distribution feeder and smart meter data obtained by the DSO.

The next section discusses some related works, the impedance modelling and geometrical determination of the cable are described in Section 3. While a numerical validation is provided in Section 4 and the results are summarised in Section 5. Finally, conclusions are given in Section 6.

2. Related works

While reflecting on the architecture of similar models on high- and medium-voltage grids, the Carson's equations are a generally accepted method for modelling the ground return path. The conventional approach for modelling the ground return path, according to Carson, is through a factitious ground conductor. In [2], Kersting presents the modified Carson's equations that have undergone the Kron reduction. Here the proposed method assumes the voltage drop over the neutral conductor to be zero, inducing that the neutral conductor does not have to be explicitly represented [8]. This is only valid in situations where the buses of the LVDS are perfectly grounded. Kron's method involves merging the neutral conductor and earth conductor which drastically reduces the calculation time according to [9, 10]. However, since the return path for (EU) low-voltage distribution networks is through a neutral conductor, different adjustments are required. This subject is well elaborated in scientific literature [3, 11–14].

The authors from [11] show that (i) the Kron reduction can only be performed for grounded neutral conductors and (ii) for some cases Carson's equations are not applicable in LVDS modelling. An error analysis has been carried out and it is observed that for a multi-grounded network, the error associated with a 4x4 matrix is acceptable (± 0.05%), having the benefit of leading to faster computation times. In this regard, they recommend viewing the earth as a single electrical point. In contrast, Koirala et al. [3] propose a new reduced impedance model to be applied on European low-voltage distribution networks. In their model, they recommend a method where the neutral conductor is insulated and the grounding occurs only at the substation and at the end user (cf. TT grounding system). The proposed impedance model allows for a more accurate power flow calculation to be obtained, which is similar to the accuracy of the alternative four-core method. On top of that, the computation time is reduced by 66%. Nevertheless, the authors in [3] use the modified Carson's equations – where a grid frequency of 60 Hz is assumed – which does not correspond to the presented European LVDS approach where the grid frequency of 50 Hz is used.

Ciric et al. [12] outlines a generic approach towards calculating the power flow in radial low-voltage distribution networks with four-core cables. They introduce an algorithm that considers the neutral ground, allowing for higher order impedance matrices to be integrated. Their approach, based on the Backward-Forward Sweep (BFS) method, clarifies that the general method can be applied to different topologies (e.g. grounded or insulated neutral).

In [13], Urquhart et al. elaborate on the implications of certain assumptions. Based on other works, they reflect on the influence of certain choices, such as (i) the consequence of working with a grounded neutral instead of an insulated one, (ii) the application of the Kron reduction on the neutral conductor currents. Their work offers a useful foundation on the choices that should be considered for certain applications. While in [14], Kotsonias et al. describe a novel approach to the previously mentioned BFS by considering the currents through the neutral conductor. Since the neutral and ground conductor will be merged in the Kron reduction, critical information about the currents flowing through the neutral conductor will be lost. Current applications of RES are often single-phase, making this information relevant for power flow calculations and (power and voltage) loss calculations, as well as neutral-point shifting [15]. Here too, accuracy will determine the computation time and thus the consideration between both must be envisaged.

Since the scope of the paper is not related to the study of electromagnetic transient behaviour in power systems, the Carson's equations are applicable. However, the Carson's equations have the following domain of validity:

1. To determine the self and mutual impedances in overhead lines. Nevertheless, it can also be applied to underground lines, though methods proposed by Sunde and Pollaczek are often more relied to due to their increased accuracy [16].
2. The earth is seen as a homogeneous solid with a constant soil resistivity (ρ). Where earth conduction effects (conduction and displacement currents) on the shunt admittance of the neutral grounding are neglected, this is only valid for power frequencies. Effects on the real soil resistivity are analysed in [17].
3. The relative permeability (ε) of the soil is considered equal to unity [18].

3. Impedance Modelling

3.1. The modified equations as presented by Kersting

According to [2], the modified Carson's equations can be written as:

$$\underline{Z}_{ii} = r_i + 0.0953 + j0.12134 \cdot \left(\ln \frac{1}{GMR_i} + 7.934 \right) \quad (1)$$

$$\underline{Z}_{ij} = 0.0953 + j0.12134 \cdot \left(\ln \frac{1}{D_{ij}} + 7.934 \right) \quad (2)$$

where:

r_i = resistance of conductor i in [Ω/mi]
GMR_i = geometric mean radius of conductor i in [ft]
D_{ij} = distance between conductors i and j in [ft]
i, j = indices representing the conductors $i \neq j \wedge i, j \in \{a, b, c, n\}$

The terms $\underline{Z}_{ii}$ and $\underline{Z}_{ij}$ represent respectively the self- and mutual impedances in [Ω/mi]. If we consider the cable segment shown in Fig. 1 as an example, the self- and mutual impedances for the phases and neutral conductors – hereafter referred to as 'a', 'b', 'c' and 'n' – can be represented as illustrated in Fig. 2.

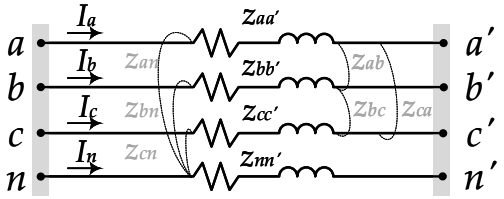

Figure 2: Self- and mutual impedance

As a result of these terms, the so called 'primitive impedance matrix' can be constructed in which diagonal elements represent the self-impedances and non-diagonal elements reflect the mutual impedances:

$$Z_{prim} = \begin{bmatrix} Z_{ii} & Z_{ij} & Z_{ij} & Z_{ij} \\ Z_{ij} & Z_{ii} & Z_{ij} & Z_{ij} \\ Z_{ij} & Z_{ij} & Z_{ii} & Z_{ij} \\ Z_{ij} & Z_{ij} & Z_{ij} & Z_{ii} \end{bmatrix}, \quad Z_{prim} \in \mathbb{C} \quad (3)$$

The matrix can then be simplified using the Kron reduction into a reduced form:

$$Z_{prim} = \begin{bmatrix} Z_{ij} & Z_{in} \\ Z_{nj} & Z_{nn} \end{bmatrix} \quad (4)$$

Finally, a 3x3 matrix is obtained in which the return path through the neutral conductor is neglected:

$$Z_{abc} = MZ_{ij} - MZ_{in} * MZ_{nj} * MZ_{nn}^{-1} \quad (5)$$

The advantage of this method, is that it reduces the computational effort and consequently the simulation time. While this is applicable to high voltage (HV) networks, adjustments are required for European LV-networks with separate neutral conductor. The modified equations (1), (2) can also be written in a decomposed form in [Ω/mi], where the angular frequency is still calculated with a frequency (f) equal to 60 Hz [2]:

$$\underline{Z}_{ii} = r_i + 4\omega P_{ii} G + j\left(X_i + 2\omega G \cdot ln \frac{S_{ii}}{RD_i} + 4\omega Q_{ii} G \right) \quad (6)$$

$$\underline{Z}_{ij} = 4\omega P_{ij} G + j\left(2\omega G \cdot ln \frac{S_{ij}}{D_{ij}} + 4\omega Q_{ij} G \right) \quad (7)$$

where:

ω = angular frequency in [rad/s]
G = constant $(0.1609347 \cdot 10^{-3})$ to convert from CGS-units to miles
X_i = reactance of conductor i in [Ω/mi]
S_{ii} = distance from conductor i to its image i' in [ft]
S_{ij} = distance from conductor i to image of conductor j in [ft]
RD_i = radius of conductor i in [ft]

With P and Q respectively the series impedance and shunt admittance correction terms, also referred to as the Carson's series. These terms represent corrections in the ground return impedance due to the imperfect earth.

3.2. Adaptations to the modified equations

This paper emphasises that these modified equations made assumptions that are not valid for European LVDS. Hereafter, an alternative is proposed, where G' replaces the used G constant. The term G' takes into account the conversion of imperial units to the metric unit system.

To obtain the alternative equations the earth resistivity (ρ) is – for convenience of comparison – also assumed to be 100 Ωm and the term G' is equal to $\cdot 10^{-4}$. Additionally, a conversion factor c is incorporated to convert the geometric parameters from [mm] to [ft]. This is necessary because the modified equations do use imperial units. Finally, as already mentioned, the frequency (f) is set to 50 Hz, resulting in:

$$\underline{Z}_{ii} = r_i + 0.049348 + j0.062832 \left(ln \frac{1}{GMR_i \cdot c} + 8.0252 \right) \quad (8)$$

$$\underline{Z}_{ij} = 0.049348 + j\ 0.062832 \left(ln \frac{1}{D_{ij} \cdot c} + 8.0252 \right) \quad (9)$$

where:

r_i = resistance of conductor i [Ω/km]
GMR_i = geometric mean radius of conductor i [mm]
D_{ij} = distance between conductors i and j [mm]
c = conversion constant $(3.28084 \cdot 10^{-3})$

Note, both (8) and (9) are expressed in [Ω/km]. Those equations are now useful in the calculation of power flows on 50 Hz grids. In [19], K. Sunderland et al. use the Carson-Clem formulae to conduct power flow analyses and reach similar results. Here, the correction term (Q) of the conductors i or j is omitted in their case. It can be concluded that the suggested adapted equations provide a more accurate solution. In an effort to investigate the influence of the assumed earth resistivity (ρ) on the impedance matrix, the authors of [20] performed a sensitivity analysis. To achieve this, they have shown that for a chosen value of ρ [10, 10000] Ωm, the error is 0.03%. Todorovski et al. [21] noted a similar observation, where for values varying between $\{10 \leq \rho \leq 10000\}\,\Omega$m an error lower than 1% is obtained. In [22] the influence of the ground resistance is discussed, which, according to them, has a large impact on the imaginary part of the impedance. [23] covers this topic as well, here the authors take the generally accepted value of 100 Ωm. Given the latter, also our work was based on the use of aforementioned value for the soil resistance.

3.3. Cable geometry determination

Primitive impedance matrices or series impedances form the foundation for modelling distribution networks. Unbalance analysis or harmonic inspection, as well as simulations of the impact RES generates on distribution networks [19, 24–27] necessitate accurate modelling of the lines in order to produce accurate results. While calculating the primitive impedance matrix, geometrical parameters are important. For instance, the geometric mean radius (GMR) and geometric mean distance (GMD, also referred to as D_{ij}) of the conductors must be known in order to solve equations (8) and (9). Often, no distinction is made in this respect between cables with round (Fig. 3, a) and sector-shaped conductors (Fig. 3, b), nor between stranded and solid cores. In spite of this, another aspect which requires attention is the presence or absence of a concentric neutral (Fig. 3, c), the latter is studied to a higher extent in [28–30]. This is due to the implications that a shield (and/or concentric neutral conductor) has on the magnetic flux and thus on the self- and mutual impedance. Such cables are less common in LV lines and more prevalent in HV-lines. As we limit ourselves to LVDS, the most common cable types are without shielding or concentric neutral. Therefore both latter cable types will not be discussed in more detail.
On the other hand, cables do not only appear in a symmetrical shape (i.e. three-core) but also in an asymmetrical shape, such as four-core cables where the distance between the conductors varies depending on whether they are horizontally/vertically adjacent or diagonally opposite one another.

Taking into account the diversity of cable constructions, a different method is recommended for estimating the GMR_i and D_{ij}. Considering a round conductor structure (as depicted in Fig. 4a and Fig. 4b), one can simply

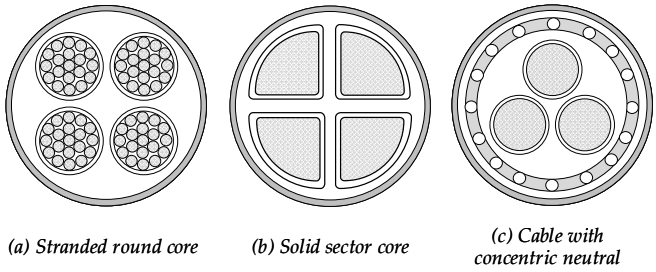

Figure 3: Diverse cable structures and geometries

formulate the geometrical mean radius and distance for horizontally/vertically adjacent and cross-adjacent conductors, using equations (10)-(13). The geometric mean radius depends, as previously mentioned, on the structure of the core (i.e. solid or stranded). Using solid cores, one defines the GMR – also designated by r' – by [31]:

$$GMR_i = e^{-\mu_r/4} \cdot r_c \;,\; r_c = \sqrt{\frac{\varnothing}{\pi}} \tag{10}$$

where r_c stands for the actual radius, which can be defined using the cross-section ($\varnothing$). The geometric mean radius can "be assumed to be a fictitious conductor without internal flux, but with the equivalent inductance compared to a conductor with radius r_c". Wherein Euler's number originates from the derivation of the internal and external flux of a conductor, as illustrated in [31]. The relative permeability (μ_r) of both copper and aluminium is weighted at 1.

As for stranded cables – frequently referred to as composite cables –, the calculation of the radius differs slightly [32]. Therefore, knowledge of the strand radius r_i is required. Values for these vary from one manufacturer to another (mostly due to economic reasons), whilst their limits are imposed by the European standard IEC EN 60228 [33]. Further, indices i and j refer to the internal strands, n the total amount of strands and d_{ij} to the distance between them. In accordance to [32], the formula for the GMR can be written as:

$$GMR = \sqrt[n]{\prod_{i=1}^{n}\left(e^{-\mu_r/4} \cdot r_i \prod_{j=1,\; j\neq i}^{n} d_{ij}\right)^{1/n}} \tag{11}$$

While parameters differ from one cable manufacturer to another and are often unavailable, the proposed methods have yielded good estimates in previous studies [23, 31].

In case of a symmetrical distribution between the conductors, i.e. in a three-core configuration, there are only horizontal or vertical adjacent conductors. Thus, the distance between conductors D_{ij} is equal and therefore equation (12) applies. Whereas an asymmetrical distribution, e.g. four-core configuration, will ensure that one distinguishes between adjacent conductors; D_{ij} and cross-adjacent conductors; D_{ij_X}. The spacing between two horizontal (or vertical) conductors is defined by considering the

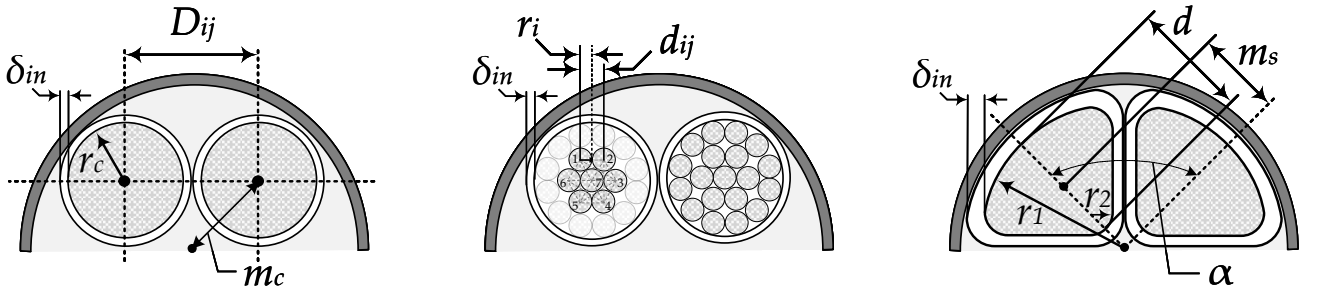

(a) Solid round cable **(b)** Stranded round cable **(c)** Sector shaped cable (based on [23])

Figure 4: Cross-sectional view of four-core cables consisting of different geometries

radius of the conductor core r_c and the insulation thickness δ_{in}:

$$D_{ij} = 2 \cdot (r_c + \delta_{in}) \tag{12}$$

Whereas for the diagonal components, using trigonometric insights, an additional term (m_c) is introduced. The term m_c denotes the distance between the centre of the round cable and the centre point of a conductor. By invoking the introduced variable, the distance for cross-adjacent components becomes:

$$\begin{aligned} m_c &= D_{ij} \cdot \frac{1}{\sqrt{2}} \\ D_{ij_X} &= 2\ m_c \end{aligned} \tag{13}$$

Notwithstanding, the structure of a stranded conductor causes the calculation of the geometrical distance D_{ij} to be more complex than that of a solid core. Note that for a conductor i with n strands, D_{ij} is calculated using the nn'^{th} root of the product of the nn'^{th} distances (d_{ij}) between the n strands of one conductor and n' strands of the other conductor:

$$D_{ij} = \sqrt[nn']{\left(d_{ii'}\ d_{ij'} \dots d_{in'}\right) \dots\ \left(d_{ni'}\ d_{nj'} \dots d_{nn'}\right)} \tag{14}$$

It is obvious that it is necessary to take into consideration the use of the insulation thickness and adhering to the trigonometrical rules in order to obtain the effects of cross-adjacent conductors, as it was also the case for the solid round conductor.

The calculation of the distance between sector-shaped conductors is studied in [23, 29, 34]. In [23], Geiss-Schroer et al. indicate that the actual value of the cross-section ($\varnothing_{real}$) can be approximated at 88% of the nominal ($\varnothing$). Moreover, the insulation thickness in LV cables is driven by mechanical strength rather than dielectric considerations [35] especially in case of small cable cross-sections. Consequently, the insulation thickness in relation to the conductor cross-section is remarkably higher for smaller sections than for larger ones. Based on the above assumption, the geometric radius of a sector-shaped conductor can be obtained from the actual cross-section:

$$GMR_i = e^{-\mu_r/4} \sqrt{\frac{\varnothing_{real}}{\pi}}\ ,\ \varnothing_{real} = 0.88\ \varnothing \tag{15}$$

Similar to round cables, the geometric mean distance can be expressed as a function of the distance from the centre point of the cable to the centre point of one conductor (m_s), see Fig. 4c. Again, the geometrical position of the conductor in relation to an adjacent conductor (i.e. horizontal/vertical or transversal) is a major determining characteristic. According to [23], the geometric mean distance between (sector-shaped) conductors depends on the conductors' angle α to the centre. The aforementioned factor is a function of the type of conductors, i.e. 3-core or 4-core cable and is represented by constant c' (respectively $\sqrt{3}$ for three-core cables and $\sqrt{2}$ for four-core cables):

$$D_{ij} = c' \cdot m_s\ ,\quad c' \in \left\{\sqrt{3},\ \sqrt{2}\right\} \tag{16}$$

Adopting the approach given in [29], the authors from [23] specify the GMD (equations (16), (19)) of two conductors by approximating the distance of their rotational axes, m_s as "the conductors rotational axis' distance to the rotational axis of the cable". Considering this, one describes m_s as:

$$m_s = r_1 - \frac{d}{2} + \theta \tag{17}$$

and due to insulation thickness, an offset factor is introduced:

$$\theta = max\left\{\frac{\delta_{in}}{\sin(\alpha/2)} - r_1 + d + r_2\left(\frac{1}{sin(\alpha/2)}\right)\ ,\ 0\right\} \tag{18}$$

where:

r_1 = back radius [mm]
r_2 = corner radius [mm]
d = sector depth [mm]
α = conductors' angle [°]
δ_{in} = insulation depth [mm]
θ = offset of the rotational axis [mm]

Finally, the distances for cross-adjacent components is given by:

$$D_{ij_X} = 2 \cdot m_s \tag{19}$$

4. Validation framework

Let us consider an existing operational LVDS as a numerical validation tool to assess the above-mentioned aspects and their impact. The studied case is limited to the impact of both (i) single-phase connected consumers and (ii) prosumers. Due to this restriction, the paper intends to consider worst-case scenarios. Consumption profiles are provided by the DSO Fluvius cvba and the profile selection is subject to a random distribution based on yearly power consumption. Further, according to the Synergrid C10/11 directive [36], the maximum authorised installed power for single-phase inverters is specified at 5 kVA. An unbiased 1:1 ratio for the creation of solar yield profiles is applied, embracing an annual consumption limit of 5.000 kWh. The lower limit is set at 1.000 kWh, in order to cover small and medium-sized end users as classified in [37]. Each node n (where $n = 1, \ldots N$) represents a single dwelling. Hence, connection cables (from cable joints to the dwelling) are in compliance with the DSO's instructions represented by a EXVB 4x16mm^2.

Depending on the geographical location, distributions networks can be distinguished in various classes, i.e. city, urban, semi-urban and rural grid topologies [38]. As a result, a city feeder consisting of 20 households is proposed for the simulations as displayed in Fig. 5. This is to compare the usage of the modified Carson's equations (1)-(2) as given by Kersting and the suggested equations (8)-(9).

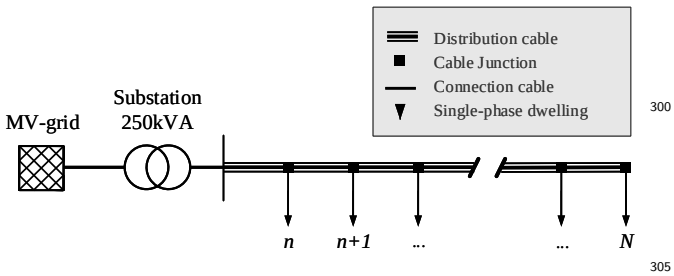

Figure 5: Graphical representation of the investigated LVDS

Grid parameters also include a variable cross-section for the distribution cable along with distinct cable geometries in contrast to the connection cable that has a fixed cross-section. This enables the study of the impact of the suggested approach within a realistic distribution feeder and to perform a sensitivity analysis for various cable cross-sections. Table 1 contains a summary of all variables used including their respective values, parameters associated with the dwellings are also listed.

Table 1: Inputs for the simulation framework

Description	Values
Grid Parameters	
Transformer rating	250 kVA
Supply voltage	3x400V + N
Cable type (distribution)	EAXeVB/AH Eca (0.6/1 kV)
Distribution cable	4x $\{50, 70, 95, 120, 150, 240\}^*$ mm^2
Cable type (connection)	EXVB Eca (0.6/1 kV)
Connection cable	4x 16 mm^2
Dwelling Parameters	
Number of dwellings	$N = 20$
Feeder length	400 m
Distance between dwellings	20 m
Length connection cable	$\urcorner[8,\ldots, 12]^\dagger$ m
Yearly consumption	$\urcorner[1000,\ldots, 5000]^\dagger$ kWh
Solar penetration	100%‡

* $\{a, b\}$ denotes a continuous uniform distribution between a and b.
† $\urcorner[a, b]$ denotes a discrete uniform distribution between a and b.
‡ The ratio of the solar yield to the annual consumption is set at 1:1, inverter losses included.

Additionally, it is assumed that the LV-feeder is part of a TT-earthing system as opposed to an actual system. Consequently, the modelling approach introduced in [3] was adopted and results are obtained using a Backward Forward Sweep (BFS, see Appendix A). The simulations do not use the Kron reduction, allowing the currents flowing through the neutral to be included.

5. Results

5.1. Error comparison for the proposed equations

For the given situation as presented in Section 4, applying the BFS algorithm with the proposed equations (8) and (9) results in Fig. 6. The voltage rise is due to the penetration of RES. In contrast, assuming there is no RES – the reverse would be observed due to the voltage drop across the lines. As the length increases, voltage variation intensifies as can be seen in the figure where the voltage rise is more pronounced at the feeder end or the longest distance from the point of common coupling. A second contributing factor is the cable section. A small cable section will offer greater resistance at the same current levels and thus cause a greater voltage drop and/or rise compared to a increased cable cross-section. Both facets are apparent in Fig. 6, whereby cables with a smaller cross-section encounter significantly higher stresses at the end of the line. Remarkably, the voltage rise for the simulations remains within the limits of the EN 50160 standard [39], where all the 10 minutes mean RMS voltages have to be within the range of U_n ±10%, i.e., 253 V and 207 V.

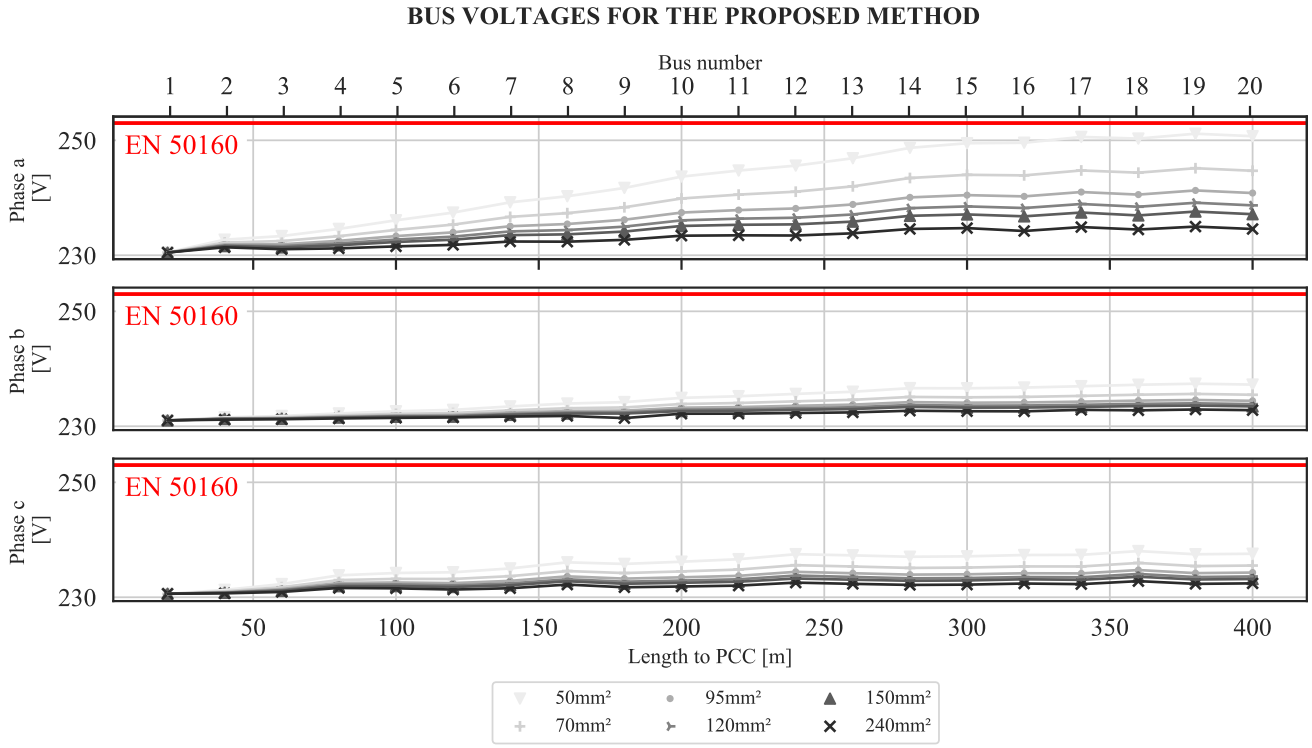

Figure 6: Voltage profile for the studied LVDS with a high degree of solar integration

While comparing the resulting absolute voltage differences between the conventional method [3] and the proposed method for different cable sections, see Fig. 7, it attracts the attention that phase a is more influenced.

This can be attributed to the internal distribution of the dwelling's phase connection and their annual consumption profile. Depending on the conductor's cross-section, a difference in absolute voltage drop/rise ΔV of more than +10V arises (cf. Fig. 7a). Once the cross-section of the conductor increases, it is less conspicuous since the resistance is sufficiently low to allow the current flow without causing a large voltage fluctuation. Moreover, smaller cross-sections will be more influenced by the frequency.

Assuming a scenario with a 50 mm² cross-section, applying the method of Koirala et al. [3] misrepresents the actual voltage profile with +4%. This may lead to voltage rises occurring in the field which are not detected in the simulation environment and may cause systems to fail (e.g. temporal disconnection of a PV-installation). Similar considerations apply to battery energy storage systems used to control the power quality of the grid, in which case the system will not be optimally modelled either.

5.2. *Effect of the cable geometry*

By comparing the three different methods, it immediately becomes apparent that both (i) the proposed methods for round and (ii) sector-shaped conductors differ slightly from each other, see Fig. 8 where the whisker boundaries represent the 5^{th} percentile and the 95^{th} percentile. This also validates the fact that both methods can be applied without compromising the accuracy of the model. Nevertheless, once again this highlights the non-acceptable deviations in results gathered by the conventional method.

5.3. *Influence of the cross-section*

Cables always have a certain insulation thickness between the conductors so that the actual distance is determined by the size of the conductor cross-section and the insulation thickness, as illustrated in Fig. 4. The latter may vary from one manufacturer to another, as derived from the IEC 60502-1 [40]. Note that these parameters are relevant for studies where both skin and proximity effects will occur. According to [41], this is only valid in case of higher cable cross-sections. Hence, the scope of this study is limited to cross-sections lower than or equal to 240 mm², since low-voltage distribution networks are restricted in cable cross-section. For increased cable cross-sections, the impact of the imaginary part of the impedance would not be negligible due to the skin effect. By limiting the scope of the paper to LVDS and excluding harmonic loads, both effects can be neglected.

5.4. *Skin, proximity and dielectric effects*

Nowadays loads need to fulfil the requirements of the IEC EN 61000-3 [42] with respect to the emissions of harmonics. Proceeding from this standard, the maximum har-

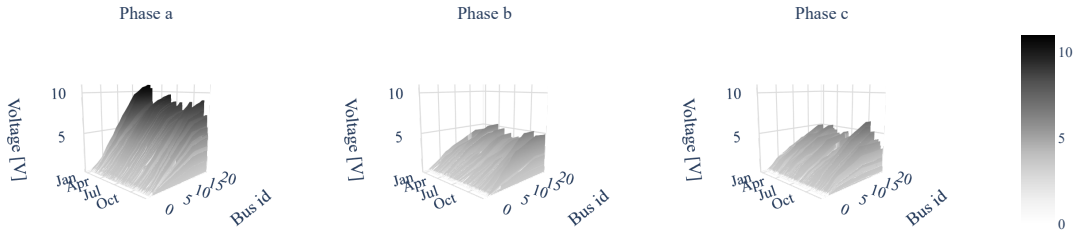

(a) Cross-section (⌀): 50mm²

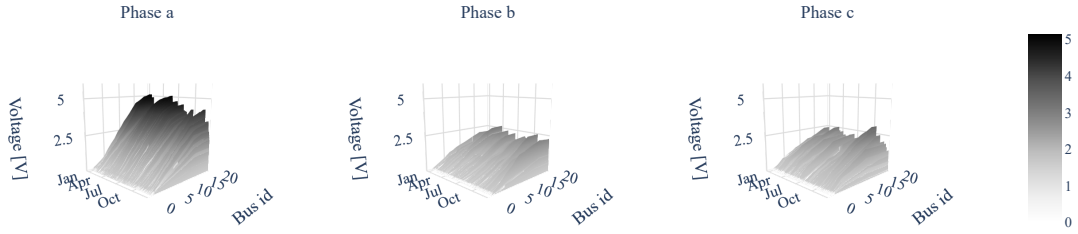

(b) Cross-section (⌀): 95mm²

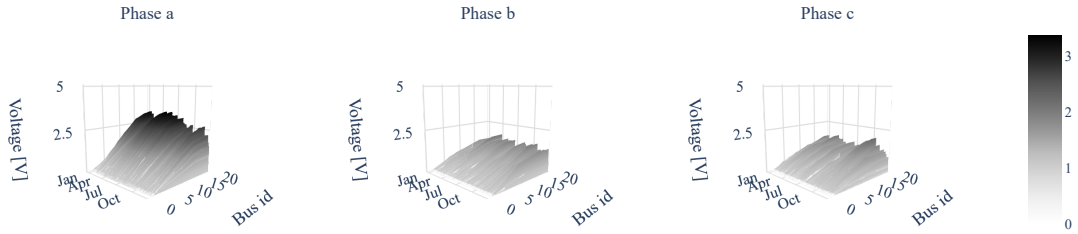

(c) Cross-section (⌀): 150mm²

Figure 7: ΔV for various cable cross-sections

monic emissions are limited to the 40^{th} order, corresponding to 2 kHz. The quarter-wavelength for this frequency range with dielectric constant $\varepsilon_r = 2.3$ for XLPE and a realistic velocity propagation in the conductor of $1.9 \cdot 10^8$ m/s, is approximatively 24.7 km. Since LVDS have an average length of 400 m, transmission line effects can be neglected. Therefore, results presented in this paper do not take harmonic loads under consideration. However, if harmonic currents occur, a more pronounced difference between the round and sector-shaped conductors shall be observed not only due to the differing geometrical properties, but also due to the increased cable resistance induced by both skin and proximity effects.

Finally, according to [43], dielectric losses can be ignored in case of buried low-voltage distribution cables since both (i) dielectric materials and (ii) voltage levels (e.g., 400 V) do not necessitate their attention. Similar assumptions are made in [2, 12, 44], where it is established that the shunt capacitances and conductances can be ignored for power system studies. While for harmonic studies, the importance of incorporating the capacitances and the shunt admittances is given in [45, 46].

6. Conclusions

This paper reviewed the key features involved in modelling the impedance of lines on LVDS in a digital twin environment. Based on existing literature, and introducing modifications where necessary, these features have been adapted to fit European low voltage grids as well. Through a reproduction of a physical feeder, the performed simulations demonstrated that the outcome of the results can be significantly affected by applying the different equations. It has been proven that the Kron reduction drastically reduces the calculation time, although it should be noted that for networks where the neutral conductor and earth conductor run separately, it cannot be used since crucial information would be lost. As a result, for applications with separate neutral conductor and PE, a 4x4 matrix must be adopted instead of a 3x3 matrix obtained via the Kron reduction.

Further it has previously been proven through a simplified network with 20 dwellings that the application of the presented method resulted in deviations of more than 4 percentage point. Such errors can have

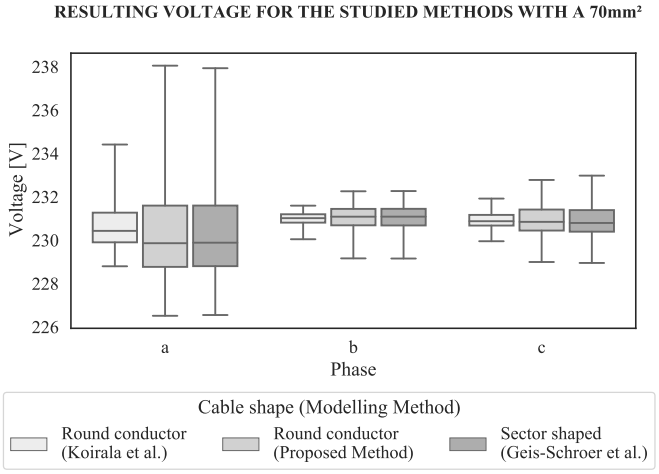

Figure 8: Result comparison of the three methods studied

major implications for the dimensioning of LVDS. Even more, such errors may lead to wrong investment choices, for example when prior simulations are made using a digital twin. Although the method has proven to be accurate, it should be noted that the validity of the assumptions are made for power system analysis without harmonics and where the soil resistivity as well as the conduction and displacement currents can be neglected.

Considering that the differences between the round and sector-shaped conductors are reasonably low, one could tolerate the use of a round conductor for calculations without sacrificing accuracy. This only applies if the simulations are limited to the voltage rises and drops in the system. Other power quality aspects (e.g. harmonics) have not been investigated in this study, but can be found in other works such as [23, 29]. Bearing in mind the great influence of the frequency on both the real and imaginary parts of the impedance, it is essential to apply the appropriate equation to obtain realistic results. This would be even more pronounced for harmonic or electromagnetic studies.

CRediT Authorship Contribution Statement

R. Cleenwerck: Conceptualization, Formal analysis, Methodology, Software, Validation, Writing- Original draft preparation, Visualization, Writing- Reviewing and Editing. **H. Azaioud:** Software, Methodology, Validation, Writing- Reviewing and Editing. **R. Claeys:** Writing- Reviewing and Editing. **T. Coosemans:** Writing- Reviewing and Editing. **J. Knockaert:** Writing- Reviewing and Editing. **J. Desmet:** Writing- Reviewing and Editing, Supervision, Funding acquisition.

Declaration of Competing Interest

The authors declare that they have no known competing financial interests or personal relationships that could have appeared to influence the work reported in this paper.

Acknowledgements

The authors would like to thank the distribution system operator Fluvius cvba for providing the anonymised dataset with consumption profiles used in this work. This research was funded by VLAIO-Flux50 ICON HBC.2018.0527 ROLECS: Roll-out of Local Energy Communities.

Appendix A. BFS Algorithm

Details of the algorithm used in the simulations is given in Table A.2.

Table A.2: Backward Forward Sweep Algorithm

Algorithm 1. Backward Forward Sweep

1: Inputs
- V_{ref} = reference voltage at LV-transformer
- N = total number of nodes
- j, k, m, n = indices for nodes and iteration count

2: Initialisation

$V_j^0 = V_{ref}\angle 0°$, $k = 1$ $\quad \forall\ j = 2, 3, \ldots N$

3: Current computation

$I_j^k = \left(\frac{P_{Lj} + jQ_{Lj}}{V_j^{(k-1)}}\right)^*$

4: Backward Sweep

$I_{nN}^k = I_N^k$

$I_{mn}^k = I_n^k + \sum\left(I_{n+1}^k \ldots I_N^k\right)$

5: Forward Sweep

$V_n^k = V_m^k - Z_{mn} \cdot I_{mn}^k$ $\quad \forall\ n = 2, 3, \ldots N$

6: Error Calculation

$e_j^k = V_j^k - V_j^{(k-1)}$, $e_{max}^k = max\left(e_j^k\right)$ $\quad \forall\ j = 2, 3, \ldots N$

7: Comparing to the tolerance ε

if $e_{max}^k \leq \varepsilon$

export results

else

$k = k + 1$

execute steps 3 … 7

References

[1] J. R. Carson, Wave propagation in overhead wires with ground return, The Bell System Technical Journal 5 (4) (1926) 539–554. doi:10.1002/j.1538-7305.1926.tb00122.x.

[2] W. H. Kersting, Distribution System Modeling and Analysis, 3rd Edition, CRC Press, Boca Raton, FL, USA, 2012. doi:10.1201/b11697.

[3] A. Koirala, R. D'hulst, D. Van Hertem, Impedance modelling for european style distribution feeder, in: 2019 International Conference on Smart Energy Systems and Technologies (SEST), IEEE, 2019, pp. 1–6. doi:10.1109/SEST.2019.8849015.

[4] A. Arshad, M. Lindner, M. Lehtonen, An Analysis of Photo-Voltaic Hosting Capacity in Finnish Low Voltage Distribution Networks, Energies 10 (11) (2017) 1702. doi:10.3390/en10111702.

[5] L. N. Ochoa, J. Quiros-Tortos, Advanced modelling of smart distribution networks using OpenDSS, in: IEEE PES ISGT Latin America 2015, IEEE, 2015.

[6] C. González-Morán, P. Arboleya, V. Pilli, Photovoltaic self consumption analysis in a european low voltage feeder, Electric Power Systems Research 194 (107087) (2021). doi:10.1016/j.epsr.2021.107087.

[7] B. Lacroix, R. Calvas, Earthing systems worldwide and evolutions, Report (2008).

[8] L. Held, F. Mueller, S. Steinle, M. Barakat, M. R. Suriyah, T. Leibfried, An optimal power flow algorithm for the simulation of energy storage systems in unbalanced three-phase distribution grids, Energies 14 (6) (2021) 1623. doi:10.3390/en14061623.

[9] T. Hubana, S. Hodzic, E. Alihodzic, A. Mulaosmanovic, The valuation of Kron Reduction application in load flow methods, Advanced Technologies, Systems, and Applications III, Springer International Publishing, 2019, pp. 70–85. doi:10.1007/978-3-030-02574-8_7.

[10] J. Zuluaga, J. Naredo, L. Castañón, M. Vega, O. Ramos-Leaños, Parallel computation of power system EMTs through Polyphase-QMF filter banks, Electric Power Systems Research 197 (2021) 107317. doi:10.1016/j.epsr.2021.107317.

[11] F. Olivier, R. Fonteneau, D. Ernst, Modelling of three-phase four-wire low-voltage cables taking into account the neutral connection to the earth, in: CIRED 2018 Ljubljana Workshop on Microgrids and Local Energy Communities, pp. 1–4. doi:10.34890/295.

[12] R. M. Ciric, A. P. Feltrin, L. F. Ochoa, Power flow in four-wire distribution networks-general approach, IEEE Transactions on Power Systems 18 (4) (2003) 1283–1290. doi:10.1109/TPWRS.2003.818597.

[13] A. J. Urquhart, M. Thomson, Assumptions and approximations typically applied in modelling LV networks with high penetrations of low carbon technologies, in: 3rd International Workshop on Integration of Solar into Power Systems, 2013.

[14] A. Kotsonias, L. Hadjidemetriou, E. Kyriakides, Power flow for a four-wire radial low voltage distribution grid with a single point grounded neutral, in: 2019 IEEE PES Innovative Smart Grid Technologies Europe (ISGT-Europe), 2019.

[15] L. Degroote, B. Renders, B. Meersman, L. Vandevelde, Neutral-point shifting and voltage unbalance due to single-phase DG units in low voltage distribution networks, in: 2009 IEEE Bucharest PowerTech, 2009, pp. 1–8. doi:10.1109/PTC.2009.5281998.

[16] T. Theodoulidis, Exact Solution of Pollaczek's Integral for Evaluation of Earth-Return Impedance for Underground Conductors, IEEE Transactions on Electromagnetic Compatibility 54 (4) (2012) 806–814. doi:10.1109/TEMC.2011.2181849.

[17] T. A. Papadopoulos, Z. G. Datsios, A. I. Chrysochos, P. N. Mikropoulos, G. K. Papagiannis, Wave Propagation Characteristics and Electromagnetic Transient Analysis of Underground Cable Systems Considering Frequency-Dependent Soil Properties, IEEE Transactions on Electromagnetic Compatibility 63 (1) (2021) 259–267. doi:10.1109/TEMC.2020.2986821.

[18] T. A. Papadopoulos, A. I. Chrysochos, C. K. Traianos, G. Papagiannis, Closed-Form Expressions for the Analysis of Wave Propagation in Overhead Distribution Lines, Energies 13 (17) (2020) 4519. doi:10.3390/en13174519.

[19] K. Sunderland, M. Coppo, M. Conlon, R. Turri, A correction current injection method for power flow analysis of unbalanced multiple-grounded 4-wire distribution networks, Electric Power Systems Research 132 (2016) 30–38. doi:10.1016/j.epsr.2015.10.027.

[20] W. H. Kersting, R. K. Green, The application of Carson's equation to the steady-state analysis of distribution feeders, in: 2011 IEEE/PES Power Systems Conference and Exposition, IEEE, 2011, pp. 1–6. doi:10.1109/PSCE.2011.5772579.

[21] M. Todorovski, R. Ackovski, Equivalent Circuit of Single-Core Cable Lines Suitable for Grounding Systems Analysis Under Line-to-Ground Faults, IEEE Transactions on Power Delivery 29 (2) (2014) 751–759. doi:10.1109/TPWRD.2013.2277887.

[22] H. Keshtkar, S. K. Solanki, J. M. Solanki, Improving the accuracy of impedance calculation for distribution power system, IEEE Transactions on Power Delivery 29 (2) (2014) 570–579. doi:10.1109/TPWRD.2013.2276061.

[23] J. Geis-Schroer, S. Hubschneider, L. Held, F. Gielnik, M. Armbruster, M. Suriyah, T. Leibfried, Modeling of german low voltage cables with ground return path, Energies 14 (5) (2021) 1265. doi:10.3390/en14051265.

[24] H. Azaioud, R. Claeys, J. Knockaert, L. Vandevelde, J. Desmet, A low-voltage DC backbone with aggregated RES and BESS: Benefits compared to a traditional low-voltage AC system, Energies 14 (5) (2021) 1420. doi:10.3390/en14051420.

[25] D. V. Bozalakov, J. Laveyne, J. Desmet, L. Vandevelde, Overvoltage and voltage unbalance mitigation in areas with high penetration of renewable energy resources by using the modified three-phase damping control strategy, Electric Power Systems Research 168 (2019) 283–294. doi:10.1016/j.epsr.2018.12.001.

[26] W. G. Chaminda Bandara, D. Almeida, R. I. Godaliyadda, M. P. Ekanayake, J. Ekanayake, A complete state estimation algorithm for a three-phase four-wire low voltage distribution system with high penetration of solar PV, International Journal of Electrical Power and Energy Systems 124 (2021) 106332. doi:10.1016/j.ijepes.2020.106332.

[27] S. Babaev, S. Cobben, V. Ćuk, H. v. d. Brom, Online estimation of cable harmonic impedance in low-voltage distribution systems, IEEE Transactions on Instrumentation and Measurement 69 (6) (2020) 2779–2789. doi:10.1109/TIM.2019.2926690.

[28] M. Shafieipour, Z. Chen, A. Menshov, J. De Silva, V. Okhmatovski, Efficiently computing the electrical parameters of cables with arbitrary cross-sections using the method-of-moments, Electric Power Systems Research 162 (2018) 37–49. doi:10.1016/j.epsr.2018.04.013.

[29] A. J. Urquhart, M. Thomson, Series impedance of distribution cables with sector-shaped conductors, IET Generation, Transmission and Distribution 9 (16) (2015) 2679–2685. doi:10.1049/iet-gtd.2015.0546.

[30] A. Hafner, M. Luz, W. Carpes Jr, Impedance and admittance calculations of a three-core power cable by the finite element method, in: International Conference on Power Systems Transients (IPST2015), Cavtat, 2015, pp. 1–8. doi:10.13140/RG.2.1.4873.5848.

[31] H. Saadat, Power system analysis, Vol. 2, McGraw-hill, 1999.

[32] A. J. Conejo, L. Baringo, Power System Components: Models, Springer International Publishing, Cham, 2018, pp. 55–96. doi:10.1007/978-3-319-69407-8_3.

[33] International Electrotechnical Commission, 60228:2004 - conductors of insulated cables, Standard, IEC, Geneva, CH (2004).

[34] M. Jensen, B. Bak-Jensen, Series impedance of the four-wire distribution cable with sector-shaped conductors, in: 2001 IEEE Porto Power Tech Proceedings (Cat. No.01EX502), Vol. 4, IEEE, 2001, pp. 6 pp. vol.4–. doi:10.1109/PTC.2001.964859.

[35] J. Desmet, Studie en analyse van de verliezen in laagspanningskabels onder harmonische belasting, Thesis (2008).

[36] Synergrid, Technisch voorschrift C10/11 ed. 2.1 - specifieke technische voorschriften voor elektriciteitsproductie-installaties die parallel werken met het distributienet, Standard (2019).

[37] R. Claeys, T. Delerue, J. Desmet, Assessing the influence of the aggregation level of residential consumers through load duration curves, in: 2019 IEEE PES Innovative Smart Grid Technologies Europe (ISGT-Europe), IEEE, 2019, pp. 1–5. doi:10.1109/ISGTEurope.2019.8905436.

[38] C. Gonzalez, J. Geuns, S. Weckx, T. Wijnhoven, P. Vingerhoets, T. De Rybel, J. Driesen, LV distribution network feeders in belgium and power quality issues due to increasing PV penetration levels, in: 2012 3rd IEEE PES Innovative Smart Grid Technologies Europe (ISGT Europe), IEEE, 2012, pp. 1–8. doi:10.1109/ISGTEurope.2012.6465624.

[39] International Electrotechnical Commission, EN 50160:2011 - voltage characteristics of electricity supplied by public distri-

bution networks, Standard, IEC, Geneva, CH (2011).

[40] International Electrotechnical Commission, EN 60502-1:2021 - power cables with extruded insulation and their accessories. part 1: Cables for rated voltages of 1 kV (Um = 1,2 kV) and 3 kV (Um = 3,6 kV), Standard, IEC, Geneva, CH (2021).

[41] J. Desmet, D. Putman, G. Vanalme, R. Belmans, D. Vandommelen, Thermal analysis of parallel underground energy cables, in: CIRED 2005 - 18th International Conference and Exhibition on Electricity Distribution, 2005, pp. 1–4. doi:10.1049/cp:20050921.

[42] International Electrotechnical Commission, EN 61000-3-SER - electromagnetic compatibility (EMC). part 3: Limit - all parts, Standard, IEC, Geneva, CH (2022).

[43] P. Caramia, G. Carpinelli, A. Russo, P. Verde, Estimation of thermal useful life of MV/LV cables in presence of harmonics and moisture migration, in: 2003 IEEE Bologna Power Tech Conference Proceedings„ Vol. 2, 2003, pp. 5 pp. Vol.2–. doi:10.1109/PTC.2003.1304300.

[44] K. M. Banjar-Nahor, F. Cadoux, K. Rauma, N. Hariyanto, N. Sinisuka, System modeling and its effect on state estimation in unbalanced low voltage networks in the presence of measurement errors, in: 2019 2nd International Conference on High Voltage Engineering and Power Systems (ICHVEPS), 2019, pp. 119–124. doi:10.1109/ICHVEPS47643.2019.9011118.

[45] V. Ćuk, J. F. G. Cobben, W. Kling, P. F. Ribeiro, Considerations on harmonic impedance estimation in low voltage networks, in: 2012 IEEE 15th International Conference on Harmonics and Quality of Power, 2012, pp. 358–363. doi:10.1109/ICHQP.2012.6381250.

[46] T. Busatto, A. Larsson, S. K. Rönnberg, M. H. J. Bollen, Including uncertainties from customer connections in calculating low-voltage harmonic impedance, IEEE Transactions on Power Delivery 34 (2) (2019) 606–615. doi:10.1109/TPWRD.2018.2881222.